SCIENTIFIC REPORTS

OPEN

SUBJECT AREAS:
QUANTUM DOTS
NANOPARTICLES

Received
18 November 2013

Accepted
23 December 2013

Published
21 January 2014

Correspondence and requests for materials should be addressed to W.F. (weifeng@tju.edu.cn)

A layer-nanostructured assembly of PbS quantum dot/multiwalled carbon nanotube for a high-performance photoswitch

Wei Feng, Chengqun Qin, Yongtao Shen, Yu Li, Wen Luo, Haoran An & Yiyu Feng

School of Materials Science and Engineering, Tianjin Key Laboratory of Composite and Functional Materials, Tianjin University, Tianjin 300072, China.

A layered nanostructure of a lead sulfide (PbS) quantum dot (QD)/multi-walled carbon nanotube (MWNT) hybrid was prepared by the electrostatic assembly after the phase transfer of PbS QDs from an organic to an aqueous phase. Well-crystallized PbS QDs with a narrow diameter (5.5 nm) was mono-dispersed on the sidewalls of MWNT by the electrostatic adsorption. Near-infrared absorption of PbS/MWNT nanostructures was improved and controlled by the packing density of PbS QDs. Efficient charge transfer between PbS and MWNT at the interface resulted in a remarkable quenching of photoluminescence up to 28.6% and a blue-shift of emission band by 300 nm. This feature was facilitated by band energy levels based on the intimate contact through the electrostatic interaction. Two-terminal devices using PbS/MWNT nanostructures showed an excellent on/off switching photocurrent and good stability during 20 cycles under light illumination due to electron transfer from PbS to MWNT. The photoswitch exhibited a high photo sensitivity up to 31.3% with the photocurrent of 18.3 μA under the light of 3.85 mW/cm^2, which outperformed many QD/carbon-based nanocomposites. Results indicate that the electrostatic layered assembly of QD/MWNT nanostructure is an excellent platform for the fabrication of high-performance optoelectronic devices.

Since the discovery, one-dimensional (1D) carbon nanotubes (CNTs) have drawn considerable attention on the design and fabrication of molecular optoelectronic nanodevices because of their unique and tunable electronic, optical and chemical properties[1–3]. Significant progresses have been made towards the preparation of a series of photo-responsive CNT-based nanocomposites such as photochromic molecules/polymers, organic fluorescent dyes and nanocrystals[4–8]. Among these, quantum dots (QDs)-anchored CNT nanohybrids combining high light-absorption and efficient charge transport based on their unique nanostructures attract an increasing amount of attention[9,10]. This nanocomposite not only enables multiple exciton generation (MEG) of QDs but also provides large QD/CNT interfaces and 1D conductive pathways favouring photo-induced charge transfer and transport[11]. Therefore, QD/CNT nanocomposites are regarded as one of ideal candidate materials for the fabrication of optoelectronic devices, such as photodetector, photoswitch and solar cells[9,12,13].

In the past few years, several strategies were presented to couple various QDs to nanotubes with different linkages[9,14–17]. One of effective coupling approaches is through the electrostatic interaction between negatively and positively charged properties of two components. Previous studies showed that the surface charges of CNTs generated by tailoring chemical structures could be tuned using different polyelectrolytes (PE)[9]. Water-dispersed PE-grafted CNTs become a hydrophilic scaffold for the surface immobilization of opposite charged QDs by the electrostatic self-assembly. The electrostatic interaction between QDs and CNTs is controlled by the diameter, dispersion, charge density and packing density of QDs on the surface of PE-grafted CNTs. Giersig et al.[18] reported the fabrication of QD/CNT heterostructures by the electrostatic interaction. Multi-walled carbon nanotube (MWNT) coated by poly(allylamine hydrochloride) (PAH) was decorated by ZnO, CdSe and CdSe-CdS nanocrystals. Nanocomposites with a highly defined morphology provided good separation and stability in aqueous solution. Zhu et al.[19] found that PAH-functioanlized MWNT electrostatically attached by CdSe QDs exhibited high electrochemiluminescence (ECL) intensity, good biocompatibility and high stability. Jia et al.[20] also presented a layer-by-layer assembly of the cationic PE-grafted MWNT with oligodeoxynucleotide-tagged CdTe QDs

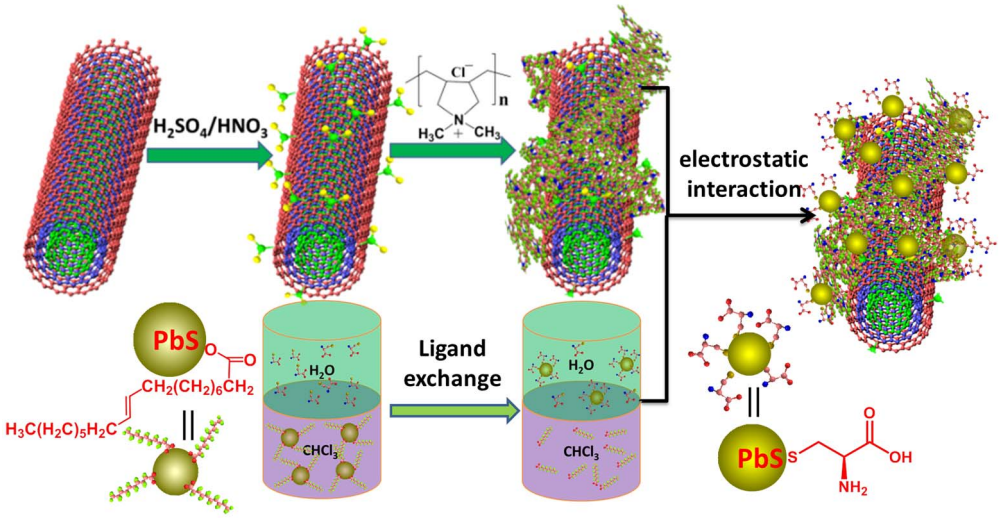

Figure 1 | Illustration of the preparation of PbS_{Cys}/MWNT nanocomposites by electrostatic interaction.

by the electrostatic interaction. This layered nanostructure delivering therapeutic genes into the nuclei of cells showed efficient intracellular transport, strong cell nucleus localization and high delivery efficiency.

Recently, a variety of UV-vis active aqueous QDs (*e.g.*, ZnO, CdSe, CdS, CdTe.) has been utilized to decorate PE-grafted CNTs by the electrostatic interaction[9,18,21]. However, near-infrared (NIR) fluorescent lead sulfide (PbS) QDs with a narrow band gap (0.41 eV) and a large exciton Bohr radius (18 nm) have hardly been incorporated into CNT-based nanocomposites by the electrostatic assembly because of the structural inhomogeneity. PbS QDs prepared in aqueous solution exhibited a long-wavelength emission, a wide size distribution and poor storage stability[22], leading to the decrease in optical properties. While monodispersed PbS QDs with good optical absorbance synthesized in colloidal organometallic solution were difficult to decorate aqueous PE-grafted CNTs because of incompatibility between two phases. The compatibility between QDs and CNTs can be improved by the phase transfer of PbS from an organic to an aqueous solution. Chemical structure controlled by the ligand exchange on the surface not only enables PbS to mono-disperse in water but also enhances the photoluminescence quantum efficiency. Wang et al.[23] showed the ligand exchange of trioctylphosphine oxide-coated QDs with polydimethylaminoethyl methacrylate homopolymers. The modified QDs are soluble in polar media and retain 70% of original photoluminescence (PL) quantum yield. Mono-dispersed PbS in an aqueous solution by the phase transfer combining a narrow size distribution and a high quantum yield can be utilized for a high-quality assembly of PbS/CNTs by the electrostatic interaction.

In this paper, a versatile noncovalent method was presented to prepare the electrostatic assembly of PbS/MWNT nanostructures after the phase transfer of PbS QDs from an organic to an aqueous solution (Figure 1). The microstructures and chemical structures of PbS QDs and PbS/MWNT hybrids were characterized by high-resolution transmission electron microscopy (HRTEM) and Fourier-transform infrared (FT-IR) spectroscopy, respectively. UV-vis-NIR absorption and PL measurement were also used to study photophysical properties. Moreover, a two-terminal device using PbS/MWNT nanostructures was fabricated. Results indicated that PbS/MWNT nanocomposites showed a switching photocurrent and good stability under the illumination of light at different intensities.

Results

Morphologies of oleic acid (OA)-capped PbS (PbS_{OA}) and L-Cysteine (Cys)-capped PbS (PbS_{Cys}) QDs were observed by TEM. Figure 2a shows that PbS_{OA} QDs prepared by a colloidal organometallic chemistry method are mono-dispersed in toluene with a diameter of 6.6 ± 0.3 nm (Figure S1), and the atomic ratio of Pb to S atoms is 29/14 according to energy dispersive X-ray spectrometry (EDS) (Figure S2). The electron diffraction (ED) pattern (the inset of Figure 2a) indicates that well-crystallized PbS shows the cubic rock salt structure, which is also confirmed by X-ray diffraction (XRD) pattern (Figure S3). HRTEM (Figure 2b) image reveals that PbS_{OA} QDs exhibit a high-crystalline structure with an interplanar distance of 0.293 nm (the inset of Figure 2b), corresponding to the (200) plane of the fcc lattice. PbS_{OA} QDs in colloidal organometallic solution were prepared using a long-time and high-temperature reaction, which facilitates the homogeneous nucleation and the growth of QDs. As a result, PbS_{OA} QDs are capped by OA ligands with a long alkyl chain, preventing QDs from being oxidzed. Thus, as-prepared PbS_{OA} QDs show a good stability and mono-dispersed size distribution.

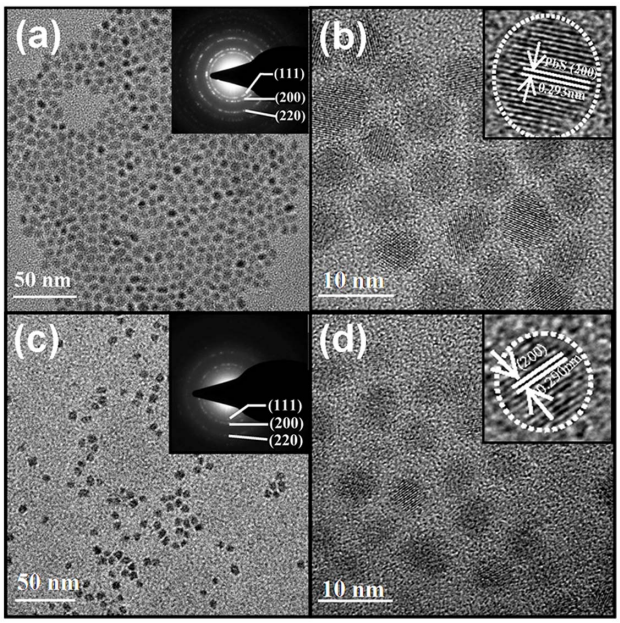

Figure 2 | TEM images of (a) mono-dispersed PbS_{OA} and (c) PbS_{Cys} QDs with the inset of corresponding fast fourier transforms (FTTs). HRTEM images of (b) PbS_{OA} and (d) PbS_{Cys} QDs with the inset of the lattice fringes of an individual QD.

TEM images of water-dispersed PbS_{Cys} QDs after the phase transfer through the ligand exchange were given in Figure 2c and 2d. PbS_{Cys} QDs also show a uniform mono-dispersion and a high-crystallinity structure (the inset of Figure 2d) after the phase transfer from toluene to water (Figure 2c). During the phase transfer, the ligands on the surface of PbS_{OA} QDs changed from OA to Cys, which thus stabilizes QDs in water with a narrow size distribution. The ligard exchange from toluene to water does not affect the dispersion of QDs and only leads to the slight variation of diameters. Compared with PbS_{OA} (6.6 ± 0.3 nm), PbS_{Cys} exhibits a decrease in diameter (5.3 ± 0.4 nm) (Figure 2d and S4). According to previous studies[24,25], the decreased size was attributed to the etching of QDs surface by the ligand exchange, during which oleic groups were replaced by Cys. Simultaneously, some Pb atoms and/or S atoms might be carried away from the core because of the replacement of OA by Cys during the phase transfer. The ligand exchange on the surface of PbS_{Cys} QDs is also confirmed by EDS (Figure S5) and the increase in atoms.

TEM images of the electrostatic assembly of PbS_{Cys}/MWNT nanocomposites were shown in Figure 3 and S6. MWNT with the diameter of 15–25 nm shows an individual dispersion due to the reduced van der Waals attraction by the surface modification. Rough surface of the sidewalls (the inset of Figure 3a) is attributed to the damage of carbon conjugated structures of nanotubes. The fracture of carbon-carbon double bonds by the oxidation of acids results in the generation of many oxygen groups such as carboxyl and carbonyl. Despite being hardly distinguished in TEM images, these side groups are useful for the electrostatic interaction between poly(diallyldimethylammonium chloride) (PDDA) and MWNT. The electrostatic assembly between negatively charged PbS_{Cys} QDs and positively charged PDDA grafted MWNT (PD-MWNT) was shown in Figure 1. Mono-dispersed PbS_{Cys} QDs with a uniform size distribution are uncovalently anchored on the sidewalls of MWNT without free QDs on the grids by the electrostatic interaction. The packing density of PbS_{Cys} QDs was tuned by the volume ratios of PbS_{Cys} to MWNT (Table 1). $PbS_{Cys}/MWNT_{5:1}$ and $PbS_{Cys}/MWNT_{1:1}$ nanocomposites were prepared by weight ratios of PbS_{Cys} to MWNT of 5 : 1 and 1 : 1, respectively. Compared with $PbS_{Cys}/MWNT_{1:1}$ (Figure 3b), $PbS_{Cys}/MWNT_{5:1}$ nanocomposite (Figure 3c) shows a remarkable increase in packing density of homogeneously dispersed QDs on MWNT because of a high proportion of PbS QDs in the assembly. The crystalline structures of PbS_{Cys} QDs were further observed by HRTEM (Figure 3d). PbS_{Cys} QDs on the sidewalls show the diameter of 5.5 nm, which is consistent with that of PbS_{Cys} QDs dispersed in water after the phase transfer. Recent works[26,27] demonstrated that the efficiency of charge transfer could be directly affected by decreasing the length of ligands, which are used to avoid the self-agglomeration. Therefore, this uniform layer-by-layer electrostatic assembly of PbS_{Cys}/MWNT with high affinity interaction facilitates charge transfer at the interface between QDs and nanotubes.

Table 1 | The detailed volumes of PbS_{Cys} and PD-MWNT solution for the electrostatic assembly

	Volume (mL)	
Nanocomposites	PbS_{Cys}[a]	PD-MWNT[b]
$PbS_{Cys}/MWNT_{5:1}$	5	1
$PbS_{Cys}/MWNT_{1:1}$	5	5

[a]The concentration of PbSCys QDs is 0.1 mg/mL.
[b]The concentration of PD-MWNT is 0.1 mg/mL.

Chemical structures of PbS QDs and PbS_{Cys}/MWNT nanocomposites were studied by FT-IR spectra. PbS_{OA} QDs (Figure 4a) show four characteristic peaks of OA including C = O stretching vibration at 1735 cm^{-1}, C-O stretching vibration at 1118 cm^{-1} and $-CH_2$ asymmetric stretching vibration at 2924 cm^{-1} and symmetric stretching vibration at 2854 cm^{-1}. Compared with PbS_{OA}, the ligand exchange from OA to Cys during the phase transfer is confirmed by a new peak at 1610 cm^{-1} and a broad peak at 1072 cm^{-1} corresponding to NH_2 deformation vibration and C-N stretching mode, respectively in PbS_{Cys} (Figure 4b). Meanwhile, no characteristic peak of S-H between 2550 and 2680 cm^{-1} indicates Cys molecules are chemisorbed as thiolates[28] by PbS QDs (Figure 4b).

The grafting of oxygen groups such as -COOH and -OH on acid-treated MWNT is indicated by several peaks including ν_{OH} at 3442 cm^{-1}, $\nu_{C=O}$ at 1654 cm^{-1}, $\nu_{C\text{-}OH}$ at 1390 cm^{-1}, δ_{OH} at 1060 cm^{-1} in Figure 4c. These groups on the sidewalls favor the electrostatic interaction between MWNT and PDDA with opposite charges. Three peaks of $-CH_2$ bending vibration at 1400 and 947 cm^{-1} and C-N stretching vibration at 1085 cm^{-1} suggest that MWNT is wrapped by PDDA by the electrostatic interaction. The attachment of PbS_{Cys} QDs on MWNT by the electrostatic self-assembly is demonstrated by multiple peaks in the curve of PbS_{Cys}/MWNT

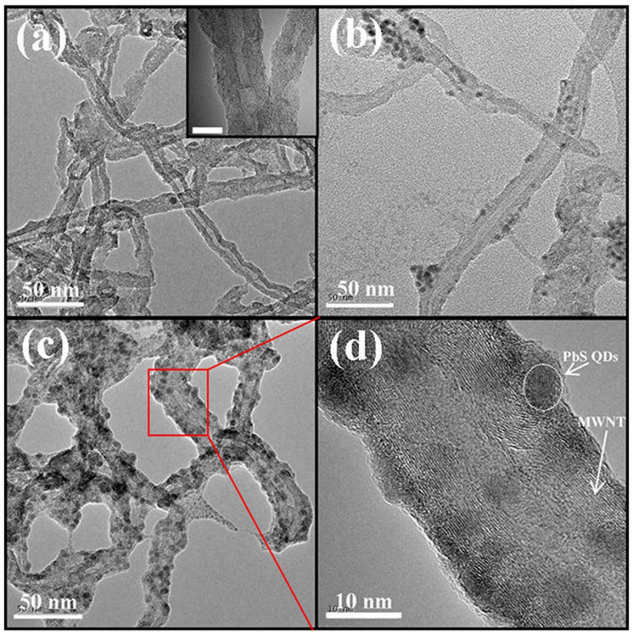

Figure 3 | TEM image of (a) Water-dispersed MWNT with the set of high resolution (scale bar is 10 nm). (b) $PbS_{Cys}/MWNT_{1:1}$ and (c) $PbS_{Cys}/MWNT_{5:1}$. (d) HRTEM image of PbS_{Cys} QDs closely attached to MWNT.

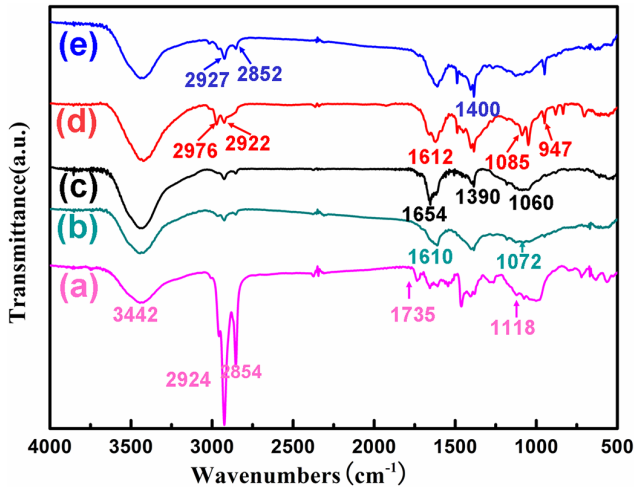

Figure 4 | FT-IR spectra of (a) PbS_{OA}, (b)PbS_{Cys} QDs, (c) MWNT, (d) PD-MWNT, and (e) PbS_{Cys}/MWNT nanocomposites.

(Figure 4e) including NH_2 deformation vibration (1610 cm^{-1}), C-OH stretching vibration (1400 cm^{-1}), $-CH_2$ bending vibration (1400 cm^{-1} and 947 cm^{-1}) and C-N stretching vibration (1072 cm^{-1}). Furthermore, asymmetric and symmetric $-CH_2$ stretching bands in PbS_{Cys}/MWNT show large red-shifts to 2927 and 2852 cm^{-1}, respectively compared with PD-MWNT at 2976 and 2922 cm^{-1}. As illustrated in previous studies, $-CH_2$ stretching vibration was an identifying indicative of the order of alkyl chains[29]. Thus, red-shifted bands of $-CH_2$ stretching indicates the increased order of alkyl chains resulting from the electrostatic adsorption of PbS_{Cys} QDs on MWNT. Results reveal that PbS_{Cys} QDs mediated by the phase transfer are anchored on the sidewalls of MWNT by the electrostatic assembly.

NIR absorption spectra of (a) PbS_{OA} in toluene, (b) PbS_{Cys} QDs, (c) $PbS_{Cys}/MWNT_{5:1}$, (d) $PbS_{Cys}/MWNT_{1:1}$ and (e) MWNT in water were shown in Figure 5. PbS_{OA} QDs with the diameter of 6.6 nm show an absorption band with the maximum peak (λ_{max}) at 1476 nm in NIR region. After the phase transfer, a dramatic blue shift of λ_{max} (1264 nm) is obtained for PbS_{Cys} QDs because of a combining effect of the decreased size of PbS_{Cys} (5.3 nm) and the change of ligands capped on the surface[24,25]. Compared with water-dispersed MWNT (Figure 5e), PbS_{Cys}/MWNT (Figure 5c and 5d) exhibits an increase in NIR absorbance in the range from 1700 to 900 nm because of the attachment of NIR-active mono-dispersed PbS_{Cys} QDs. However, the absorption edge and the peak of band of PbS_{Cys} QDs are not distinguished clearly in the NIR region for two curves of PbS_{Cys}/MWNT nanocomposites. This band-edgeless absorption was also observed in a series of QDs attached on the surface of CNTs including CdSe[18], PbS[27] and CdS[31]. According to previous studies, this result was attributed to the charge diffusion or electronic interaction between QDs and MWNT in the ground state at the interface. The featureless band-edge absorption in NIR region was an indicative of intimate contact between PbS_{Cys} QDs and MWNT, which enables efficient photo-induced interfacial charge transfer.

Furthermore, NIR absorption of PbS_{Cys}/MWNT can be further tuned by packing density of PbS_{Cys} QDs on the surface of MWNT. It can be seen that NIR absorption of $PbS_{Cys}/MWNT_{5:1}$ nanocomposite is higher than that of $PbS_{Cys}/MWNT_{1:1}$ due to high density of PbS_{Cys} QDs on the sidewalls. Moreover, PbS_{Cys} (Figure 5b) and PbS_{Cys}/MWNT (Figure 5c and 5d) in water exhibit small bumpers around 1500–1800 nm owing to strong water resonance, which is hardly eliminated by measuring the baseline[30]. This analysis is confirmed by the result that no bumper is found in the absorption of PbS_{OA} QDs in toluene (Figure 5a).

Figure 6 displays PL spectra of (a) PbS_{OA} in toluene, (b) PbS_{Cys} QDs, (c) $PbS_{Cys}/MWNT_{5:1}$ and (d) $PbS_{Cys}/MWNT_{1:1}$ in water. PbS_{OA} QDs shows a strong emission peak (λ_{em}) at 1554 nm (Figure 6a). Compared with PbS_{OA}, a remarkably reduced intensity of λ_{em} at 1309 nm with a blue-shift by 245 nm is observed in PbS_{Cys} QDs (Figure 6b). According to previous studies[24,32], PL intensity showed a strong surface dependence and thus was sensitive to the structure of ligands. Furthermore, during the phase transfer, oxidative etching of QD surface occurred because of the existence of oxygen in solution[25]. Consistent with NIR absorption, the blue-shifted emission band arises from combining effects of the decreased size from 6.6 to 5.3 nm, the re-distribution of electronic density and the increased confinement energy, resulting from the formation of strong Pb-thiol bond on QDs by the ligand exchange[33]. Moreover, when anchored on the surface of MWNT, PbS_{Cys} QDs show a remarkable quenching of blue-shifted luminescence. It can be seen that PL intensity at λ_{em} of $PbS_{Cys}/MWNT_{5:1}$ and $PbS_{Cys}/MWNT_{1:1}$ decrease by 20.3% and 28.6% respectively compared with PbS_{Cys} QDs. Strong quenching of PL is attributed to the presence of alternative nonradiative decay pathways favoring charge transfer from the conductive band of PbS QDs (donor) to the empty electronic state of MWNT (acceptor) at the interface[18,21,34]. Charge transfer from PbS_{Cys} QDs to MWNT is facilitated by their respective band energy levels (Figure 7d) based on the intimate contact through the electrostatic interaction. The interaction is also confirmed by a blue-shifted emission band of PbS_{Cys}/MWNT nanocomposites. The λ_{em} of $PbS_{Cys}/MWNT_{5:1}$ and $PbS_{Cys}/MWNT_{1:1}$ blue-shift to 1027 and 1009 nm responsively from 1309 nm of PbS_{Cys} QDs. This blue-shifted emission bands of QD/MWNT nanocomposites are consistent with the reports by Wang et al.[25,35] recently. PbS QDs capped with the oleylamine ligands attached on the surface of MWNT exhibit a remarkable blue-shift of emission band due to the electronic interaction between PbS and MWNT at the interface. In our hybrid, PbS_{Cys} QDs are absorbed on the surface of MWNT by the electrostatic interaction between the ligands and PDDA. As a result, the blue-shifted band is attributed to the electronic interaction between PbS_{Cys} and MWNT by changing electronic density and the confinement energy of PbS_{Cys} rather than decreased QDs sizes. TEM images show that PbS_{Cys} QDs decorated on MWNT shows the diameter of 5.5 nm, which is the same to that of dispersed PbS_{Cys} in water after the phase transfer. This analysis is also confirmed by the result that

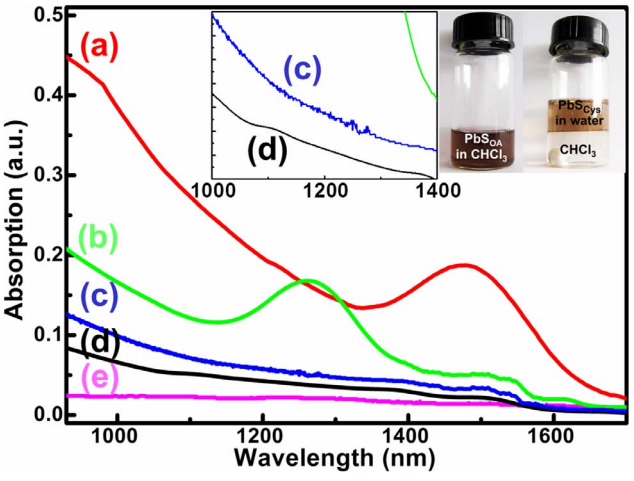

Figure 5 | NIR absorption spectra and of (a) PbS_{OA} in toluene, (b) PbS_{Cys} QDs, (c) $PbS_{Cys}/MWNT_{5:1}$, (d) $PbS_{Cys}/MWNT_{1:1}$, and (e) MWNT in water with the inset of enlarged spectra at the corresponding wavelength. Top inset: optical images of PbS_{OA} QDs (left) in toluene, and (right) in water after the phase transfer.

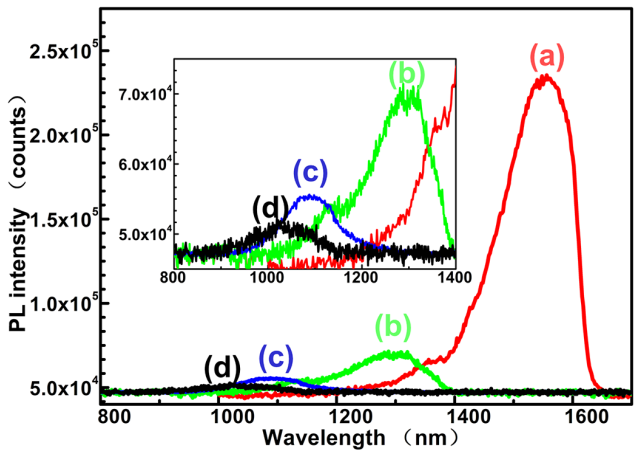

Figure 6 | PL spectra of (a) PbS_{OA} in toluene, (b) PbS_{Cys} QDs, (c) $PbS_{Cys}/MWNT_{5:1}$, and (d) $PbS_{Cys}/MWNT_{1:1}$ in water under the excitation of visible light at 465 nm. Inset shows the enlarged spectra at the corresponding wavelength.

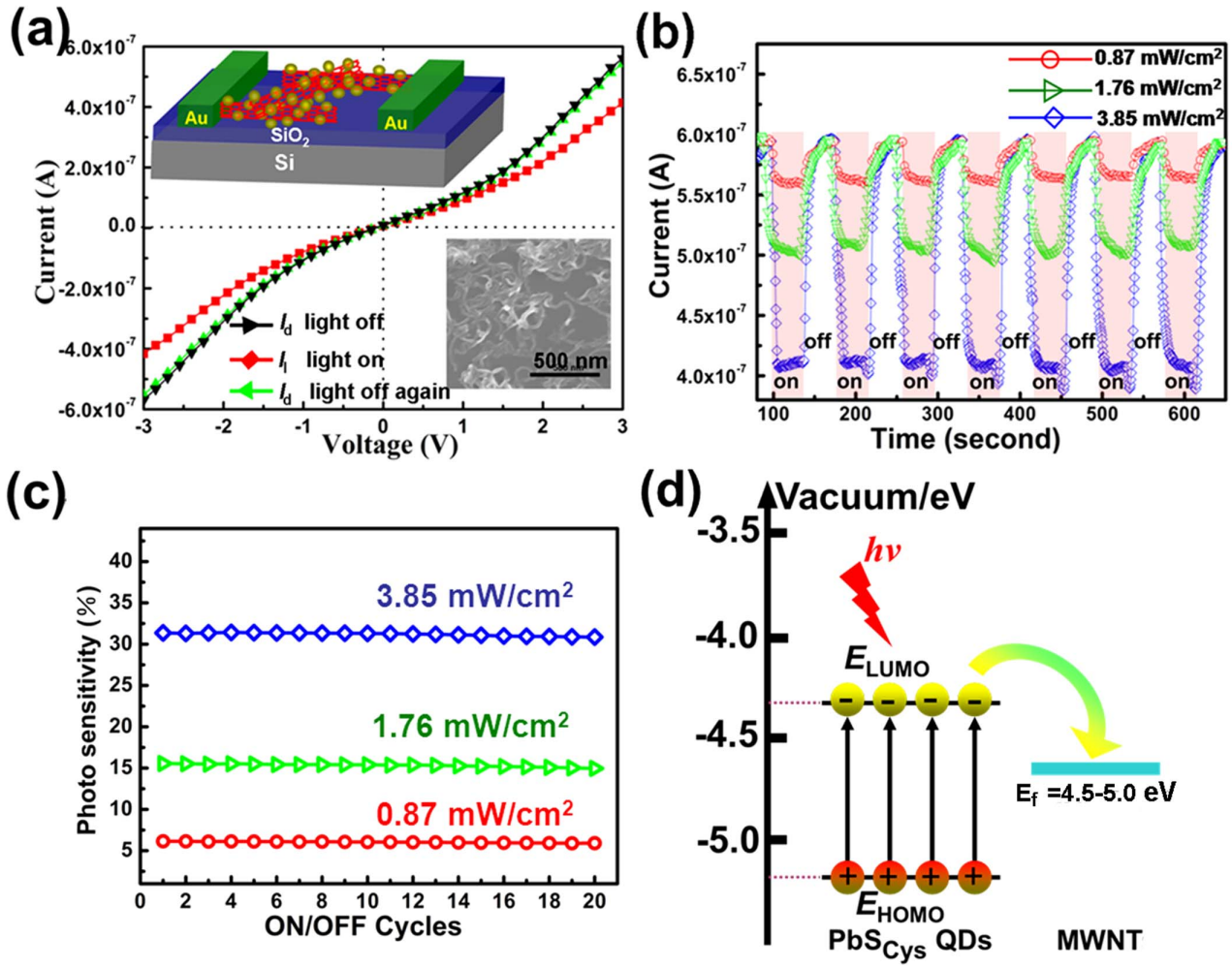

Figure 7 | Photoresponse of a two-terminal device based on $PbS_{Cys}/MWNT_{5:1}$ nanocomposites. (a) Representative *I-V* curves of $PbS_{Cys}/MWNT_{5:1}$ in dark and under light irradiation of 2.03 mW/cm^2. Top left inset: scheme illustration of a two-terminal device and right bottom inset: SEM image of $PbS_{Cys}/MWNT_{5:1}$ deposited on a Si/SiO_2 substrate. (b) Photocurrent response of a photoswitch during seven ON/OFF cycles under light irradiation of 0.87, 1.76 and 3.85 mW/cm^2. (c) Photo sensitivity of a photoswitch during 20 cycles under light irradiation of 0.87, 1.76 and 3.85 mW/cm^2. (d) Energy level diagram adjusted in relation to the vaccum level of PbS_{Cys}/MWNT hybrid. Arrow indicates electron transfer from PbS to MWNT under light illumination.

$PbS_{Cys}/MWNT_{5:1}$ with no changes in QDs size exhibits a larger blue-shift of λ_{em} than that of $PbS_{Cys}/MWNT_{1:1}$.

Discussion

Photoresponse of a two-terminal photoswitch based on $PbS_{Cys}/MWNT_{5:1}$ hybrid was investigated by drop-casting hybrid solution onto source/drain channels on a Si/SiO_2 (450 nm) substrate. Schematic depiction of a two-terminal device was shown in upper inset of Figure 7a. SEM image (the right bottom inset of Figure 7a) displays 3D interconnected networks of $PbS_{Cys}/MWNT_{5:1}$ in the channel of devices, favoring charge mobility from source/drain to gate. Figure 7a shows typical current-voltage (*I-V*) curves of $PbS_{Cys}/MWNT_{5:1}$ nanocomposites in dark and under light irradiation of 2.03 mW/cm^2. Compared with *I-V* response in dark, a remarkable decrease in current is obtained under light illumination. The decreased current returns to its initial value in dark when the light is switched off. Previous studies demonstrated that the device based on pure MWNT with the same structure shows no increase in photocurrent when the light was switched on/off[11,31]. Thus, the decrease in photocurrent of $PbS_{Cys}/MWNT_{5:1}$ nanocomposite arises from the photo-induced electron transfer between PbS and MWNT. Photoactive on/off switching characteristics of the device under light irradiation of 0.87, 1.76 and 3.85 mW/cm^2 at 2 V source-drain bias (V_{ds}) was further studied in Figure 7b. The light was turned on and off for 40 s. Each cycle of the current consists of three transient regimes – a sharp decrease and constant state under the illumination and a fast relaxation to dark value when the light is off. The response (light on) and recovery time (light off) of photocurrent in every cycle are shown in Figure S7. $PbS_{Cys}/MWNT_{5:1}$ nanocomposite exhibits a slight increase in response time and recovery time as the increasing number of cycles. The response time of $PbS_{Cys}/MWNT_{5:1}$ irradiated by the light of 3.85 mW/cm^2 changes from 9.0 s (the first cycle) to 12.9 s (the tenth cycle). The increasing response time of photocurrent upon cycling was also observed by previous studies[15,36,37]. It also can be seen that the response time and recovery time of $PbS_{Cys}/MWNT_{5:1}$ irradiated by the light of 1.76 and 3.85 mW/cm^2 is longer than that of 0.87 mW/cm^2. This result indicates that a great amount of electrons is not excited and transfers to MWNT at the interface by a low-intensity light. Thus, the photoresponse of PbS_{Cys}/MWNT can be adjusted by the output energy of irradiation light.

Figure 6b shows that the on/off switching current was tuned by the intensity of light illumination. Photocurrent (I_{ph}) and photo sensitivity (*P*) are evaluated by the equation (1) and (2), respectively.

$$I_{ph} = |I_l - I_d| \quad (1)$$

$$P = I_{ph}/I_d \times 100\% \quad (2)$$

where I_d is the current in dark, and I_l is the current under illumination. As shown in Figure 7c, $PbS_{Cys}/MWNT_{5:1}$ exhibits an increase in photo sensitivity under illumination of light at a high power density. Specifically, the photoswitch shows a high I_{ph} of 18.3 μA and P up to 31.3% under the light of 3.85 mW/cm^2 compared with 3.5 μA and 6.0% at 0.87 mW/cm^2. Moreover, the device holds a good reversibility and cycling stability of photoresponse. Photo sensitivity shows no decay during 20 cycles under illumination of light at three intensities. Photoresponse and cycling performance of $PbS_{Cys}/MWNT_{5:1}$ outperform many QD/carbon-based nanocomposites reported[13,14,32]. The stable and reversible photoresponse tuned by light intensity is critical for high-performance sensors and rewritable memory devices.

Generally, the increase in I_{ph} of the switch using QD/CNT nanocomposites was mainly attributed to charge transfer between QDs and CNTs at the interface. In this work, the delocalized electron-hole pairs over PbS QDs created by incident light excitation dissociate at the interface between PbS and MWNT[38]. This interaction results in electron transfer from PbS to MWNT[11,15], which is facilitated by the intimate contact between QDs and nanotubes by the electrostatic assembly. Thus, electron-hole recombination on the nanotube (hole transporter) reduces I_l due to the decreased hole concentration in MWNT network, leading to the increase in I_{ph}. Besides, according to previous studies[11,16], holes in PbS QDs could also be annihilated by the reaction in the environment. Electrostatic interaction (gate effect) between PbS and MWNT drives nanotubes into off-state, which also contributes to the decrease in I_l. The analysis is confirmed by the result that I_{ph} is tuned by illuminated light of different densities. Excited by a high-density light, an increasing amount of electron-hole pairs is generated for the dissociation and transfer at the interface between PbS and MWNT. Thus, more electrons created by PbS_{Cys} are recombined and annihilated by holes on the nanotubes, resulting in a lower hole concentration. Meanwhile, the gate effect is also significant under illumination of light at high density. Consequently, combining effects of hole recombination and gate effect result in a remarkable increase in I_{ph}.

Electron transfer in PbS_{Cys}/MWNT nanocomposites is illustrated by band energy diagram (Figure 7d). The lowest unoccupied molecular orbital (LUMO) energy of PbS_{Cys} QDs is -4.32 eV calculated according to reference[37,39], and band gap is 0.86 eV from the formula reported by Hens et al.[40], and thus the highest occupied molecular orbital (HOMO) level is -5.18 eV. The favorable energy band alignment is advantageous to exciton dissociation and transfer at the interface. Under illumination, electron in the ground state of PbS transits to the excited state by absorbing photons. Electron-hole pairs formed on the surface of QDs dissociated at the interface. Electron transfer from PbS to MWNT (Fermi level is 4.5~5.0 eV) is facilitated by band gap offsets. Therefore, hole concentration in MWNT is remarkably decreased by electron-hole recombination, which affects hole transport through the nanotube network and thus leads to the increase in I_{ph}. Results indicate that an electrostatic assembly of PbS_{Cys}/MWNT nanocomposites shows an excellent photoresponse and good cycling performance due to favorable charge transfer at the interface. This QD/CNT nanostructure can be developed for high-performance photoswitches by optimizing the electrostatic interaction between QDs and nanotubes.

Conclusion

Well-crystallized PbS_{Cys} QDs after the phase transfer from toluene to water were uncovalently attached onto PD-MWNT by the electrostatic assembly. The packing density of PbS_{Cys} was controlled by tuning the weight ratios of QDs to MWNT. PbS_{Cys}/MWNT nanocomposites displayed an improved NIR absorption because of the presence of uniform mono-dispersion of PbS QDs on the sidewalls. Compared with PbS_{Cys}, a remarkable quenching of PL (28.6%) and a blue-shifted (300 nm) band of PbS_{Cys}/MWNT indicated the efficient charge transfer between PbS and MWNT at the interface. This result was further investigated by a two-terminal device based on PbS/MWNT nanostructures. Under light illumination, photo-induced electron transfer from PbS to MWNT resulted in an excellent on/off switching photocurrent and good stability during 20 cycles. $PbS_{Cys}/MWNT_{5:1}$ nanocomposite showed a high photo sensitivity up to 31.3% with the photocurrent of 18.3 μA under the light of 3.85 mW/cm^2, which outperformed many QD/carbon-based nanocomposites. This work paves a way for the fabrication of high-performance optoelectronic devices using the electrostatic layered assembly of PbS/MWNT nanostructures.

Methods

Materials. Raw MWNT was purified by the mild oxidation in H_2O_2 solution[41] and treated in the mixture of sulfuric acids and nitric acids to generate many oxygen-groups on the sidewalls. Water-dispersed MWNT was obtained after rinsing with distilled water for several times by filtration until pH of filtrate is 7. Lead (II) acetate trihydrate ($Pb(OAc)_2$), OA, and thioacetamide (Alfa Aesar) were used as received, and Cys, Tri-n-octylphosphine (TOP), tetramethylammonium hydroxide pentahydrate (TMAH), and PDDA (20%, w/w, in water, Mw = 200000–350000) were purchased from Sigma-Aldrich. All other reagents were used without further purification.

Synthesis of OA-capped PbS QDs. PbS_{OA} QDs were synthesized by an organometallic chemistry method[42]. Typically, $Pb(OAc)_2$ (0.91 g, 2.4 mmol), OA (2.8 mL, 8.2 mmol), diphenylether (8 mL, 50.3 mmol) and distilled TOP (4 mL, 9.0 mmol) were mixed at room temperature. The mixture was purged by nitrogen and heated at 90°C for 1 h. Subsequently, the sulphur-precursor solution of thioacetamide (0.64 g, 0.88 mmol) and TOP (4.8 mL, 10.8 mmol) in 0.4 mL of N,N-Dimethylformamide was added to the above mixture at 90°C. The reaction was carried out for 12 h at 100°C. The resultant products were washed with isopropyl alcohol by centrifugation to remove residual precursors. PbS_{OA} QDs were dispersed in toluene to form a uniform solution (3 mg/mL).

Synthesis of aqueous Cys-capped PbS QDs by the phase transfer. The phase transfer of PbS_{OA} QDs into a water solution was carried out by the ligand exchange[43]. Cys (121.16 mg, 1 mmol) and TMAH (360 mg, 2 mmol) were dissolved in 10 mL of methanol to form a CTMA salt as a phase transfer agent. PbS_{OA} QDs toluene solution (0.5 mL) was added to 5 mL of chloroform. While stirring, 0.5 mL of CTMA solution was added dropwise to the PbS_{OA} QDs solution, and ultrapure water (5 mL) was also added as an aqueous solvent at a reduced stirring speed. QDs were transferred to the upper aqueous phase after a few minutes and further purified with acetone by centrifugation and re-dispersed in ultrapure water. The resulting aqueous PbS_{Cys} QDs (Yield: 80%) were obtained.

Synthesis of PbS_{Cys}/MWNT by the electrostatic self-assembly. Water-dispersed MWNT (5.0 mg) was dispersed in 200 mL of water by ultrasonication for 1 h. PDDA (0.5 mL) as a cationic PE, 0.5 M NaCl and 1.0 M NaOH were mixed in uniform MWNT dispersion by ultrasonication for 5 h. MWNT was encapsulated by PDDA by the electrostatic interaction. PD-MWNT with positive charges on the surface and good stability in an aqueous solution (0.5 mg/mL) was acquired after removing excessive PDDA by washing with di-water for several times via centrifugation. PbS_{Cys}/MWNT nanocomposite with a layered nanostructure was prepared by the electrostatic self-assembly at room temperature as shown in Figure 1. Typically, 5 mL of negative charged PbS_{Cys} QDs (0.1 mg/mL) solution was added to a certain volume (1 mL or 5 mL) of positively charged PD-MWNT solution at a concentration of 0.1 mg/mL (Table 1). The weight ratios of PbS_{Cys} to MWNT were 5 : 1 and 1 : 1 for $PbS_{Cys}/MWNT_{5:1}$ and $PbS_{Cys}/MWNT_{1:1}$, respectively. The total volume of the solution was 10 mL by adding ultrapure water. The mixture was ultrasonicated for 10 min, and the electrostatic interaction was carried out for 30 min under stirring. The resultant layered assembly of PbS_{Cys}/MWNT hybrid was gained after removing excess QDs by subsequent centrifugation and rinse with di-water for several times. Of particular were the PL measurements, which were performed on unpurified hybrid samples at the same concentration of QDs.

Fabrication of the device. A two-terminal device (photoswitch) was fabricated as follows: An n-type Si wafer with a 450 nm thick layer of thermally grown SiO_2 dielectric was used as the substrate. Conventional photolithography process was performed to fabricate the microelectrode plate by patterning Au contact pads on top of the substrates. Si/SiO_2 substrate was ultrasonically rinsed in distilled water, alcohol and acetone successively and dried with a nitrogen gun. PbS_{Cys}/MWNT nanocomposite was dispersed in di-water to form a uniform solution. This hybrid solution was drop-casted on the surface of SiO_2. The device was dried and stored in vacuum.

Characterization. The microstructures of PbS QDs and PbS_{Cys}/MWNT hybrid were observed by HRTEM (Tecnai G2 F20). FT-IR spectroscopy was carried out on a Bruker Tensor 27 spectrometer to analyze chemical structures. UV-vis-NIR absorption and PL were studied by a spectrophotometer (UV-3600, Shimadzu) and a spectroflurometer (FL3-221-TCSPC, HORIBA Jobin Yvon Inc), respectively. Morphologies of PbS_{Cys}/MWNT hybrids on the substrate of the photoswitch were observed by field-emission scanning electron microscopy (FESEM, Hitachi S-4800).

The device was irradiated by a 150 W halogen lamp (Beijing Changtuo Technology Company). This light source delivered a continuous spectrum ranging from 200 to 2000 nm. The incident white light was focused and guided by a long optical fiber to avoid the heating effect, and the power intensity delivered on the photoswitch was measured using the light density meter (Beijing Zhongjiaojinyuan Co., Ltd.). Photoswitching properties upon light irradiation with different power densities were recorded by keithley 4200-SCS and a micromanipulator 6150 probe station in a clean and shielded box at room temperature in air.

1. Iijima, S. Helical Microtubules of Graphitic Carbon. *Nature*, **354**, 56–58 (1991).
2. Misewich, J. A., Martel, R., Avouris, P., Tsang, J. C., Heinze, S. & Tersoff, J. *et al.* Electrically induced optical emission from a carbon nanotube FET. *Science* **300**, 783–783 (2003).
3. Hao, F. *et al.* High electrocatalytic activity of vertically aligned single-walled carbon nanotubes towards sulfide redox shuttles. *Sci. Rep.* **2**, 368 (2012).
4. Feng, W., Luo, W. & Feng, Y. Y. Photo-responsive carbon nanomaterials functionalized by azobenzene moieties: structures, properties and application. *Nanoscale* **4**, 6118–6134 (2012).
5. Li, L. *et al.* Electrochemiluminescence energy transfer-promoted ultrasensitive immunoassay using near-infrared-emitting CdSeTe/CdS/ZnS quantum dots and gold nanorods. *Sci. Rep.* **3**, 1529; DOI:10.1038/srep01529 (2013).
6. Alvaro, M., Aprile, C., Ferrer, B. & Garcia, H. Functional molecules from single wall carbon nanotubes. Photoinduced solubility of short single wall carbon nanotube residues by covalent anchoring of 2,4,6-Triarylpyrylium units. *J. Am. Chem. Soc.* **129**, 5647–5655 (2007).
7. Yang, Z. *et al.* Controllable synthesis of fluorescent carbon dots and their detection application as nanoprobes. *Nano-Micro Lett.* **5**, 247–259 (2013).
8. Gebhard, T. Injector quantum dot molecule infrared photodetector: a concept for efficient carrier injection. *Nano-Micro Lett.* **3**, 121–126 (2011).
9. Peng, X. H., Chen, J. Y., Misewich, J. A. & Wong, S. S. Carbon nanotube-nanocraytal heterostructures. *Chem. Soc. Rev.* **38**, 1076–1098 (2009).
10. Ravindran, S., Chaudhary, S., Colburn, B., Ozkan, M. & Ozkan, C. S. Covalent coupling of quantum dots to multiwalled carbon nanotubes for electronic device applications. *Nano Lett.* **3**, 447–453 (2003).
11. Li, X. L., Jia, Y. & Gao, A. Y. Tailored single-walled carbon nanotube-CdS nanoparticle hybrids for tunable optoelectronic devices. *ACS Nano* **4**, 506–512 (2009).
12. Zhang, G. Q. & Lou, X. W. D. Controlled Growth of $NiCo_2O_4$ Nanorods and Ultrathin Nanosheets on Carbon Nanofibers for High-performance Supercapacitors. *Sci. Rep.* **3**, 1470; DOI:10.1038/srep01470 (2013).
13. Chaudhary, S., Kim, J. H., Singh, K. V. & Ozkan, M. Fluorescence microscopy visualization of single-walled carbon nanotubes using semiconductor nanocrystals. *Nano Lett.* **4**, 2415–2419 (2004).
14. Sheeney-Haj-Khia, L., Basnar, B. & Willner, I. Efficient generation of photocurrents by using CdS/carbon nanotube assemblies on electrodes. *Angew. Chem. Int. Ed.* **44**, 78–83 (2005).
15. Hu, L. B. *et al.* Light-induced charge transfer in Pyrene/CdSe-SWNT hybrids. *Adv. Mater.* **20**, 939-946 (2008).
16. Juárez, B. H., Klinke, C., Kornowski, A. & Weller, H. Quantum dot attachment and morphology control by carbon nanotubes. *Nano Lett.* **7**, 3564–3568 (2007).
17. Yu, K. H. *et al.* Controllable photoelectron transfer in CdSe nanocrystal-carbon nanotube hybrid structures. *Nanoscale* **4**, 742–746 (2012).
18. Olek, M., Büsgen, T., Hilgendorff, M. & Giersig, M. Qauntum dot modified multiwall carbon nanotubes. *J. Phys. Chem. B* **110**, 12901–12904 (2006).
19. Jie, G., Li, L. L., Chen, C., Xuan, J. & Zhu, J. J. Enhanced electrochemiluminescence of CdSe quantum dots composited with CNTs and PDDA for sensitive immunoassay. *Biosens. Bioelectron.* **24**, 3352–3358 (2009).
20. Jia, N. Q. *et al.* Intracellular delivery of quantum dots tagged antisense oligodeoxynucleotides by functionalized multiwalled carbon nanotubes. *Nano Lett.* **7**, 2976–2980 (2007).
21. Jeong, S., Shim, H. C., Kim, S. & Han, C. S. Efficient Electron transfer in functional assemblies of pyridine-modified NQDs on SWNTs. *ACS Nano* **4**, 324–330 (2009).
22. Bakueva, L. *et al.* PbS quantum dots with stable efficient luminescence in the near-IR spectral range. *Adv. Mater.* **16**, 926–929 (2004).
23. Wang, X. S. *et al.* Surface passivation of luminescent colloidal quantum dots with poly(Dimethylaminoethyl methacrylate) through a ligand exchange process. *J. Am. Chem. Soc.* **126**, 7784–7785 (2004).
24. Zhao, H. G., Wang, D. F., Chaker, M. & Ma, D. L. Effect of different types of surface ligands on the structure and optical property of water-soluble PbS quantum dots encapsulated by amphiphilic polymers. *J. Phys. Chem. C* **115**, 1620–1626 (2011).
25. Lin, W. J. *et al.* Highly luminescent lead sulfide nanocrystals in organic solvents and water through ligand exchange with poly(acrylic acid). *Langmuir* **24**, 8215–8219 (2008).
26. Tang, J. *et al.* Colloidal-quantum-dot photovoltaics using atomic-ligand passivation. *Nat. Mater.* **10**, 765–771 (2011).
27. Wang, D. F. *et al.* Controlled fabrication of PbS quantum-dot/carbon-nanotube nanoarchitecture and its significant contribution to near-infrared photon-to-current conversion. *Adv. Funct. Mater.* **21**, 4010–4018 (2011).
28. Xu, D., Liu, Z. P., Liang, J. B. & Qian, Y. T. Solvothermal synthesis of CdS nanowires in a mixed solvent of ethylenediamine and dodecanethiol. *J. Phys. Chem. B* **109**, 14344–14349 (2005).
29. Sandhyarani, N. & Pradeep, T. Crystalline solids of alloy clusters. *Chem. Mater.* **12**, 1755–1761 (2000).
30. Hyun, B. R., Chen, H. Y., Rey, D. A., Wise, F. W. & Batt, C. A. Near-infrared fluorescence imaging with water-soluble lead salt quantum dots. *J. Phys. Chem. B* **111**, 5726–5730 (2007).
31. Robel, R., Bunker, B. A. & Kamat, P. V. Single-walled carbon nanotube–CdS nanocomposites as light-harvesting assemblies: photoinduced charge-transfer interactions. *Adv. Mater.* **17**, 2458–2463 (2005).
32. Hinds, S. *et al.* NIR-emitting colloidal quantum dots having 26% luminescence quantum yield in buffer solution. *J. Am. Chem. Soc.* **129**, 7218–7219 (2007).
33. Shukla, S. *et al.* Polymeric nanocomposites involving a physical blend of IR sensitive quantum dots and carbon nanotubes for photodetection. *J. Phys. Chem. C* **114**, 3180–3184 (2010).
34. Shim, H. C., Jeong, S. & Han, C. S. Controlled assembly of CdSe/MWNT hybrid material and its fast photoresponse with wavelength selectivity. *Nanotechnology* **22**, 165201 (2011).
35. Wang, D. F., Zhao, H. G., Wu, N. Q., Khakani, M. A. & Ma, D. L. Tuning the charge-transfer property of PbS-quantum dot/TiO_2-nanobelt nanohybrids via quantum confinement. *J. Phys. Chem. Lett.* **1**, 1030–1035 (2010).
36. Cheng, S. *et al.* All Carbon-Based Photodetectors: An eminent integration of graphite quantum dots and two dimensional graphene. *Sci. Rep.* **3**, 2694; DOI:10.1038/srep02694 (2013).
37. Zhang, D. Y. *et al.* Understanding charge transfer at PbS-decorated graphene surfaces toward a tunable photosensor. *Adv. Mater.* **24**, 2715–2720 (2012).
38. Sargent, E. H. Infrared photovoltaics made by solution processing. *Nat. Photonics* **3**, 325–331 (2009).
39. Jasieniak, J. *et al.* Luminescence and amplified stimulated emission in CdSe-ZnS-nanocrystal-doped TiO_2 and ZrO_2 waveguides. *Adv. Funct. Mater.* **17**, 1654–1662 (2007).
40. Moreels, I. *et al.* Size-dependent optical properties of colloidal PbS quantum dots. *ACS Nano* **3**, 3023–3030 (2009).
41. Feng, Y. Y. *et al.* Room temperature purification of few-walled carbon nanotubes with high yield. *ACS Nano* **2**, 1634–1638 (2008).
42. Nagel, M., Hickey, S. G., Fromsdorf, A., Kornowski, A. & Weller, H. Synthesis of monodisperse PbS nanoparticals and their highly ordered 3D colloidal crystals. *Z. Phys. Chem.* **221**, 427–437 (2007).
43. Wei, Y. F., Yang, J. & Ying, J. Y. Reversible phase transfer of quantum dots and metal nanoparticles. *Chem. Commun.* **46**, 3179–3181 (2010).

Acknowledgments

This work was financially supported by the National Basic Research Program of China (Grant no. 2012CB626800 and 2010CB934700), the National Natural Science Foundation of China (Grant no. 51073115, 51273144 and 51373116), the Research Fund for the Doctoral Program of Higher Education of China (Grant no. 20110032110067) and Program for New Century Excellent Talents in University (NCET-13-0403).

Author contributions

F. W. and F. Y. Y. conceived the project. Q. C. Q., S. Y. T. and L. Y. performed the experiment and characterization of materials. Q. C. Q. and F. Y. Y. wrote the paper and analyzed the results. L. W. and A. H. R. help the analysis of some results.

Additional information

Supplementary information accompanies this paper at http://www.nature.com/scientificreports

Competing financial interests: The authors declare no competing financial interests.

How to cite this article: Feng, W. *et al.* A layer-nanostructured assembly of PbS quantum dot/multiwalled carbon nanotube for a high-performance photoswitch. *Sci. Rep.* **4**, 3777; DOI:10.1038/srep03777 (2014).